ACS Chemical Neuroscience

pubs.acs.org/chemneuro Research Article

Simulated Performance of Electroenzymatic Glutamate Biosensors In Vivo Illuminates the Complex Connection to Calibration In Vitro

Mackenzie Clay and Harold G. Monbouquette*

Cite This: *ACS Chem. Neurosci.* 2021, 12, 4275–4285 Read Online

ACCESS | Metrics & More | Article Recommendations

ABSTRACT: Detailed simulations show that the relationship between electroenzymatic glutamate (Glut) sensor performance in vitro and that modeled in vivo is complicated by the influence of both resistances to mass transfer and clearance rates of Glut and H_2O_2 in the brain extracellular space (ECS). Mathematical modeling provides a powerful means to illustrate how these devices are expected to respond to a variety of conditions in vivo in ways that cannot be accomplished readily using existing experimental techniques. Through the use of transient model simulations in one spatial dimension, it is shown that the sensor response in vivo may exhibit much greater dependence on H_2O_2 mass transfer and clearance in the surrounding tissue than previously thought. This dependence may lead to sensor signals more than double the expected values (based on prior sensor calibration in vitro) for Glut release events within a few microns of the sensor surface. The sensor response in general is greatly affected by the distance between the device and location of Glut release, and apparent concentrations reported by simulated sensors consistently are well *below* the actual Glut levels for events occurring at distances greater than a few microns. Simulations of transient Glut concentrations, including a physiologically relevant bolus release, indicate that detection of Glut signaling likely is limited to events within 30 μm of the sensor surface based on representative sensor detection limits. It follows that important limitations also exist with respect to interpretation of decays in sensor signals, including relation of such data to actual Glut concentration declines in vivo. Thus, the use of sensor signal data to determine quantitatively the rates of Glut uptake from the brain ECS likely is problematic. The model is designed to represent a broad range of relevant physiological conditions, and although limited to one dimension, provides much needed guidance regarding the interpretation in general of electroenzymatic sensor data gathered in vivo.

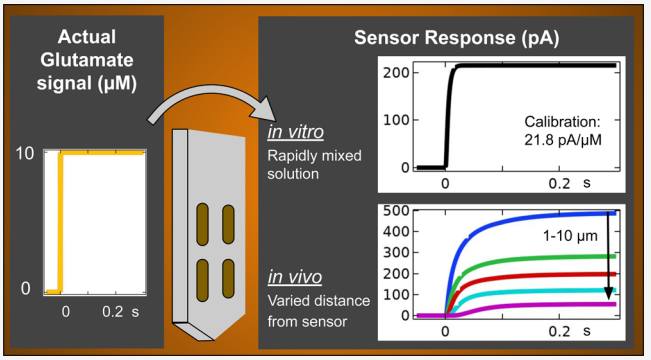

KEYWORDS: *glutamate, glutamate biosensor, mathematical model, neurochemical sensing in vivo, glutamate sensing in vivo, sensor spatiotemporal resolution in vivo*

1. INTRODUCTION

Electroenzymatic microsensors have proven valuable for the selective monitoring of nonelectroactive chemical species including glutamate (Glut), glucose, ATP, acetylcholine, and choline in the deep brain.[1−7] These biosensors are based on one or more immobilized enzymes that serve as the selective recognition element (s) and that generate an electroactive species, commonly H_2O_2, which is oxidized or reduced at an underlying electrode to give a current signal. The electrode is normally coated with one or more permselective polymer layers to prevent electroactive interfering compounds, such as ascorbic acid (AA), from accessing the electrode surface. For example, in the case of Glut sensors, glutamate oxidase (GlutOx) is commonly immobilized onto a polymer-coated electrode surface using a cross-linking compound such as glutaraldehyde. The immobilized enzyme catalyzes the oxidation of Glut to produce H_2O_2, which may then diffuse through the permselective film (s) to the electrode surface where it is electrooxidized to produce a measurable current signal, usually in the picoamp to nanoamp range. The current produced is a function of the ambient Glut concentration, and the biosensor response is often reported as a concentration measurement that is calculated using a calibration factor, which is determined in vitro prior to sensor use.

Historically, the primary competing technology for deep-brain sensing has been microdialysis. Microdialysis may be employed to detect virtually any neurochemical for which an

Received: June 3, 2021
Accepted: October 12, 2021
Published: November 4, 2021

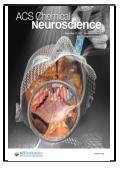

https://doi.org/10.1021/acschemneuro.1c00365
ACS Chem. Neurosci. 2021, 12, 4275–4285

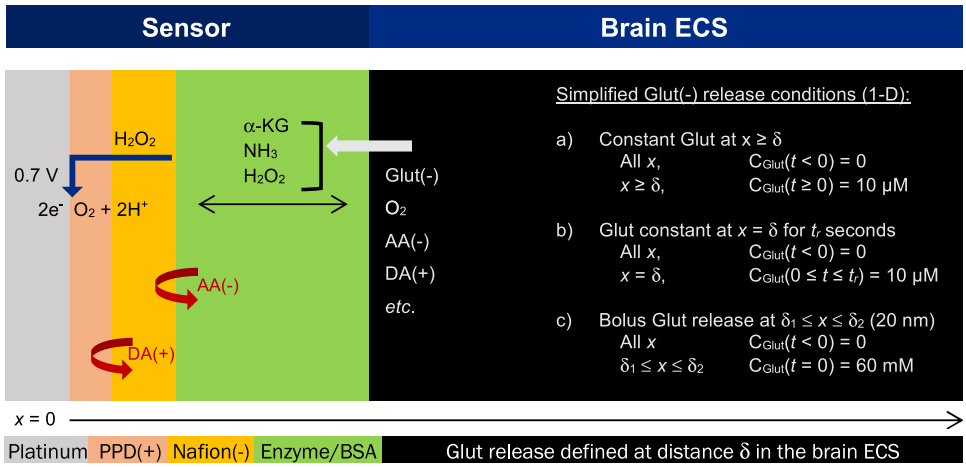

Figure 1. Sensor schematic and the set of conditions used to model Glut release into the brain ECS. Equations 1 and 2 (see Section 3) describe the diffusion and reaction of Glut, O_2, and H_2O_2 within each 1-D domain (PPD, Nafion, enzyme/BSA, and brain ECS). AA, DA, α-ketoglutarate, NH_3, and H^+ are not modeled.

analytical technique exists, including high-performance liquid chromatography, mass spectrometry, capillary electrophoresis, and so on, whereas electroenzymatic sensors have been developed only for the small set of analytes for which appropriate enzymes are available. The typical tradeoffs have been the relatively large size of implanted microdialysis devices and their relatively poor temporal resolution, although some recent technical advances in microdialysis and related "push-pull" microdevices have reduced these disadvantages.[8,9]

Of late, genetically encoded fluorescent sensors for neurochemicals, including Glut, have emerged as a very different and powerful approach to follow the activity of hundreds of neurons simultaneously.[10−13] However, extensive implementation of the technique is complicated by the limited, mm-scale penetration depth of visible light in the brain, requiring the use of fiber-optic probes or implantable miniaturized microscopes (i.e., miniscopes) to monitor the emitted light from deep-brain regions.[14] Also, genetically encoded sensors are available for a limited number of analytes, and the design of biosensors with a sufficiently high binding constant to detect species at low concentration, yet exhibiting rapid enough dissociation rates to track transient neurotransmitter signaling, presents an ongoing challenge.

The clear advantages and disadvantages of these primary approaches for monitoring neurochemicals in vivo suggest that each will have a role going forward in elucidating brain function. In particular, electroenzymatic sensors are well suited to deep-brain measurements where good spatiotemporal resolution and minimal tissue damage are vital. A recent electroenzymatic Glut sensor design offers a several-fold improvement in sensitivity to 320 nA μM^{-1} cm^{-2} and an order-of-magnitude improvement in intrinsic response time (in the absence of external mass transfer resistance) to ~80 ms,[15] which adds to the appeal of the technology.

However, even the fastest electroenzymatic sensors exhibit response times that are too slow to monitor true synaptic neurotransmitter dynamics, which occur on the millisecond to sub-millisecond time scale. As with microdialysis probes, analysis of time-dependent electroenzymatic sensor data is further complicated by neurochemical mass transfer rates and clearance mechanisms in the brain, which limit sensor sampling space and can mask neurotransmitter signal characteristics.[16] These considerations highlight the need to formulate validated approaches for the interpretation of electroenzymatic sensor data to better establish the true usefulness of these tools for the study of transient neurological processes.

A central issue is the applicability of calibration factors obtained in vitro, typically by measuring sensor responses to step changes in concentration administered in a rapidly stirred beaker, for interpretation of sensor data gathered in vivo. To date, use of electroenzymatic sensors to study neurotransmitter concentrations has been predicated on the assumption that these biosensors will perform the same in both environments and that the rise and decay of signals from implanted sensors are straightforwardly reflective of corresponding concentration changes in vivo. However, the environments employed for calibration where external mass transfer is minimized or essentially eliminated are not reflective of the relatively quiescent deep brain environment where external mass transfer limitations cannot be ignored. A previous theoretical and experimental study of glucose and hypoxanthine biosensors addressed differences in sensor performance in a stirred beaker, in agar, and in brain tissue.[17] In brain tissue, Newton et al. found that the lack of convective mass transfer to quickly transport analytes to the biosensor surface combined with the presence of H_2O_2 clearance mechanisms resulted in a steady-state sensor response of only ~1.5% of that expected for the same bulk concentration in a stirred beaker.[17] The influence of diffusional mass transfer resistance on the implanted sensor response was recognized and modeled many years ago,[18] and significant improvements were made to the early analytical approach in an effort to better describe experimental dopamine (DA) sensor data gathered in vivo.[19] Although aspects of these earlier models have been adopted in this work, the goal here is to illustrate the complicated relationship between the responses of electroenzymatic Glut sensors calibrated in vitro and clearly defined, transient Glut release events in the simulated brain.

To understand better how Glut sensors perform in the complex environment of the brain, a simulation strategy using a validated model of an ideal Glut biosensor coupled with an accepted mathematical description of diffusive mass transport and sensible ranges of average Glut and H_2O_2 uptake and clearance rates is applied here for a clearly defined set of Glut release scenarios at various distances from the biosensor.

https://doi.org/10.1021/acschemneuro.1c00365
ACS Chem. Neurosci. 2021, 12, 4275−4285

Although the transient, one-dimensional model employed is an approximation, it is known to be a reasonably good one for the description of transport to typical sensors with characteristic dimension >25 μm.[20] The sensor parameters used in this study correspond to a theoretically optimized design of the sort shown in Figure 1 with a sensitivity of 364 nA μM^{-1} cm^{-2} and a response time of 8 ms, whereas the best measured intrinsic response time (in the absence of external mass transfer resistance) is ~80 ms.[15] These simulation results therefore correspond to aspirational sensor performance metrics, yet they illustrate well the key issues encountered in the interpretation of sensor data in what may be the best-case scenario. Of course, these findings apply best to Glut biosensors of the particular design described here, yet they are expected to be qualitatively valid for electroenzymatic sensors of related construction.

2. RESULTS AND DISCUSSION

2.1. Model Development and Simulated Sensor Response to Glut Concentration Step Changes in the Brain Extracellular Space (ECS). A detailed, transient mathematical model in one spatial dimension (1-D) was developed to provide an approximate description of Glut sensor performance in vivo and to study the sensitivity of simulation results to parameters describing the clearance rate of Glut and H_2O_2 from the brain ECS. This model builds upon a previously published mathematical description of sensor performance in vitro under conditions where external mass transfer resistance is minimal[15,21] to include an additional, brain ECS domain where the rates of chemical diffusion to and from the sensor as well as the biological clearance rates of Glut and H_2O_2 are included. These rates of external mass transfer and clearance are generally not considered when a Glut sensor is calibrated in a stirred beaker, yet they play an important role in sensor performance in vivo. The importance of these considerations was demonstrated previously by reported simulations of and experiments with electroenzymatic sensors implanted in a gel or tissue and exposed to constant bulk analyte concentration.[17]

However, an understanding of the sensor response to transients in neurotransmitter concentrations as well as the influence of varied clearance and uptake rates within the ECS clearly is of central importance for the interpretation of sensor data used to study actual brain function. Noting that many of the properties affecting the clearance of neurochemicals from the ECS are expected to vary from one region to another, as well as over time, the model simulations presented here were run over a range of reasonable values (Table 1) to capture the effects of temporal and spatial variability in the brain (see Section 3). However, modeling in 1-D has some intrinsic limitations, including those pertaining to the description of neurotransmitter release. For example, the difference between synaptic dimensions and sensor sites (~40−150 μm) cannot be addressed in 1-D models that describe only linear distances such as the depth into sensor coatings, not the surface area of the sensor itself. Nevertheless, diffusive transport to the sensors considered in this simulation study is expected to be modeled well in 1-D, because their characteristic dimension is assumed to exceed 25 μm.[20]

Table 1. First-Order Rate Constants for Glut Uptake and H_2O_2 Clearance (s^{-1})

species	slow	moderate	fast
Glut	4.33 s^{-1}	4.95 s^{-1}	7.7 s^{-1}
H_2O_2	0.0116 s^{-1}	5 s^{-1}	30 s^{-1}

Because sensor calibration in vitro normally is conducted by recording sensor responses to step changes in Glut concentration, initial simulations were conducted for step changes to 10 μM Glut at various distances, δ, from the sensor in the simulated ECS (Figure 1a). A Glut concentration of 10 μM was chosen because it appears to be representative of the peak concentration observed in the mammalian ECS.[22] Because Glut concentration changes are expected to originate at a variety of finite distances from an implanted sensor surface, the step change was specified at a varied distance from the sensor to assess how well sensors may describe a well-defined change in concentration beyond their immediate vicinity in vivo.

In order for calibration factors obtained from data gathered in vitro to be useful directly, sensor responses to actual Glut concentrations in the simulated ECS should be predictable by applying straightforwardly such calibration factors to the recorded current signals. For the simulations shown in Figure 2 and elsewhere in this study, the sensor is characterized by a calibration factor of 21.85 pA/μM for Glut concentrations within the linear range of the sensor. Somewhat unexpectedly, simulations predict that when a step change in concentration occurs close to the sensor surface (<3 μm away), sensor current signals correspond to apparent concentrations (based on the calibration factor) that are as much as twofold (or more) greater than the actual imposed concentration of 10 μM in the release zone (Figure 2). For step changes in concentration more distant from the sensor surface, the sensor response is predicted to be reduced significantly relative to that expected for a sustained 10 μM release, dropping to 25% of the expected response for Glut release at a distance of 10 μm and

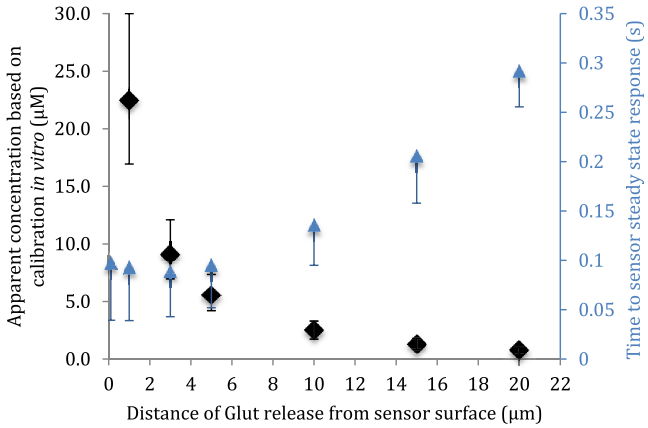

Figure 2. Simulated biosensor response in vivo to a 10 μM step change in Glut concentration at various distances for moderate Glut and H_2O_2 clearance rates. Apparent concentration measurements were calculated using the calibration factor (21.85 pA/μM) obtained in vitro. The time periods required for the approximate steady-state responses represent the time to 90% of the actual steady-state values, consistent with calibration procedures in vitro (see text). Error bar termini correspond to the slow and fast biological clearance rates of Glut and H_2O_2 given above (see Section 3) where slower rates result in higher sensitivities and longer response times. Steady-state response times for the slowest H_2O_2 clearance rate (for any Glut uptake rate) are omitted because achievement of steady state required >80 s.

https://doi.org/10.1021/acschemneuro.1c00365
ACS Chem. Neurosci. 2021, 12, 4275−4285

to below 7.6% of the expected response for Glut released at 20 μm. For the simulated range of Glut and H_2O_2 clearance rates, the sensor response is greater for slower rates and lower for faster rates, as described by the error bars in Figure 2. These simulations show that the relationship between sensor performance in vitro, in the absence of external mass transfer limitations and Glut and H_2O_2 clearance mechanisms, and in a simulated brain environment is not straightforward.

The large deviations in the simulated sensor response from what might be expected (Figure 2) arise from the significant mass transfer resistance to species transport to and away from the sensor surface in vivo as well as chemical clearance mechanisms in the brain ECS. A rapidly stirred beaker often is used for calibrations in vitro, which minimizes mass transfer resistances between the sensor and bulk fluid. Stirring results in rapid convective transport of Glut and O_2 to the sensor surface and rapid removal of typically most H_2O_2 produced in the sensor enzyme layer. It is important to note that the Glut concentration at the sensor surface never achieves the concentration released (10 μM in this case) as the simulated system approaches steady state whether in vivo or in vitro. The sensor response is related to the rate of Glut transport to the sensor, the rate of Glut uptake in the brain, the rate of Glut turnover in the GlutOx layer of the sensor, and ultimately, the delivery of H_2O_2 to the Pt electrode surface where H_2O_2 is electrooxidized to give rise to the current signal. For example, for a Glut step change to 10 μM at 5 μm from the sensor in vivo, a sensor surface concentration of <2.6 μM provides the driving force for Glut diffusion to the sensor surface at the steady state and a current signal corresponding to a bulk concentration of ~6 μM Glut (based on in vitro calibrations). Because resistance to mass transport of H_2O_2 from the sensor surface also is greater in vivo, a greater fraction of H_2O_2 produced may be transported to the Pt electrode surface, which can give rise to larger sensor current signals in vivo than expected (Figure 2) when Glut release events occur very close to the sensor surface. Representative concentration profiles for Glut, H_2O_2, and O_2 both within the sensor coatings and the brain ECF at the steady state for Glut release maintained at 10 μM at 5 μm from the sensor surface are shown in Figure 3. Note that the slopes of the concentration profiles at the sensor surface provide an indication of the diffusive mass transfer rates of the chemical species between the sensor surface and the simulated ECS.

Prior simulations of sensor calibration in vitro (using the same sensor parameters but including convective mass transfer at the sensor surface and a mass transfer coefficient of 0.05 cm/s for H_2O_2) indicate that only ~15% of the H_2O_2 arising from Glut oxidation catalyzed by GlutOx immobilized in the sensor surface layer diffuses to the underlying Pt electrode where it is electrooxidized to give a current signal; most of the H_2O_2 diffuses to the sensor surface where it is flushed away rapidly to the bulk solution by convective mass transfer.[15,21] In the brain, mass transfer of H_2O_2 from the sensor surface to the ECS occurs primarily by much slower diffusion, augmented somewhat by biological mechanisms that clear H_2O_2 at relatively slow rates. H_2O_2 clearance results primarily from catalase activity and the glutathione system and exhibits characteristic times ranging from 0.1 s to minutes.[23−25] Nevertheless, the slower removal rates of H_2O_2 can lead to not only higher sensor signals in vivo than expected from calibrations in vitro (as mentioned above), but also to a moderate accumulation of H_2O_2 in the brain in the vicinity of the sensor. However, this H_2O_2 accumulation is not expected to show any toxic effects unless it well exceeds 10 μM.[26] For moderate rates of H_2O_2 clearance (5 s^{-1}), the highest accumulation of H_2O_2 for the simulated sensor responses shown in Figure 2 is 10 μM (faster and slower expected clearance rates result in peak concentrations of 7.25 and 13.5 μM, respectively) for Glut release at 1 μm, and in all cases, this value drops by ~60% or more for release 3 μm or greater from the sensor surface. The sensor response scales with H_2O_2 concentration at the electrode surface, which can be elevated for Glut release events closest to the sensor surface that give rise to local H_2O_2 accumulation.

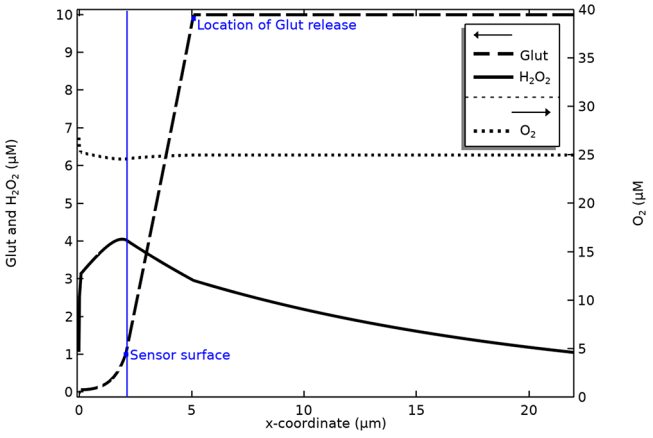

Figure 3. Steady-state concentration profiles after a 10 μM step change in Glut 5 μm from the sensor surface. The sensor surface is located at x = 2.093 μm, and the underlying platinum electrode within the sensor is located at x = 0. H_2O_2 concentration decreases asymptotically to 0 for x > 2.093 μm. The x-coordinate is the distance from the Pt electrode surface underlying the permselective films and the immobilized enzyme layer of the sensor.

The intrinsic response time for these sensors is defined in accordance with common practice in the field, namely, the time required for the sensor to reach 90% of the steady-state response to a step change in bulk Glut concentration in a system where external mass transfer resistance between the sensor and the bulk solution essentially is eliminated (by rapid stirring for example). The simulations presented here (Figure 2) suggest that much longer times generally are required to approach steady state in vivo, typically >90 ms versus 8 ms in vitro for an ideal optimized sensor of the design shown in Figure 1,[15] depending on sensor proximity to the Glut source and H_2O_2 clearance rate. This order-of-magnitude difference between the simulated sensor response in vivo and the intrinsic sensor response time also arises from the slow rate of diffusive transport between the brain and the sensor surface. When Glut release occurs very close to the sensor surface, within a few microns, for example, the steady-state Glut concentration profile over this small distance sets up quickly, whereas the H_2O_2 profile, which extends tens of microns into the brain, approaches its steady-state character much more slowly. Thus, H_2O_2 mass transfer and clearance rates may be expected to control the apparent response of the sensor in vivo. For example, for Glut release <1 μm from the sensor surface, the simulated Glut profile becomes constant after ~10 ms, whereas the H_2O_2 concentration profile approaches steady state at ~100 ms, thereby controlling the apparent sensor response. H_2O_2 mass transfer and clearance become progressively less

https://doi.org/10.1021/acschemneuro.1c00365
ACS Chem. Neurosci. 2021, 12, 4275−4285

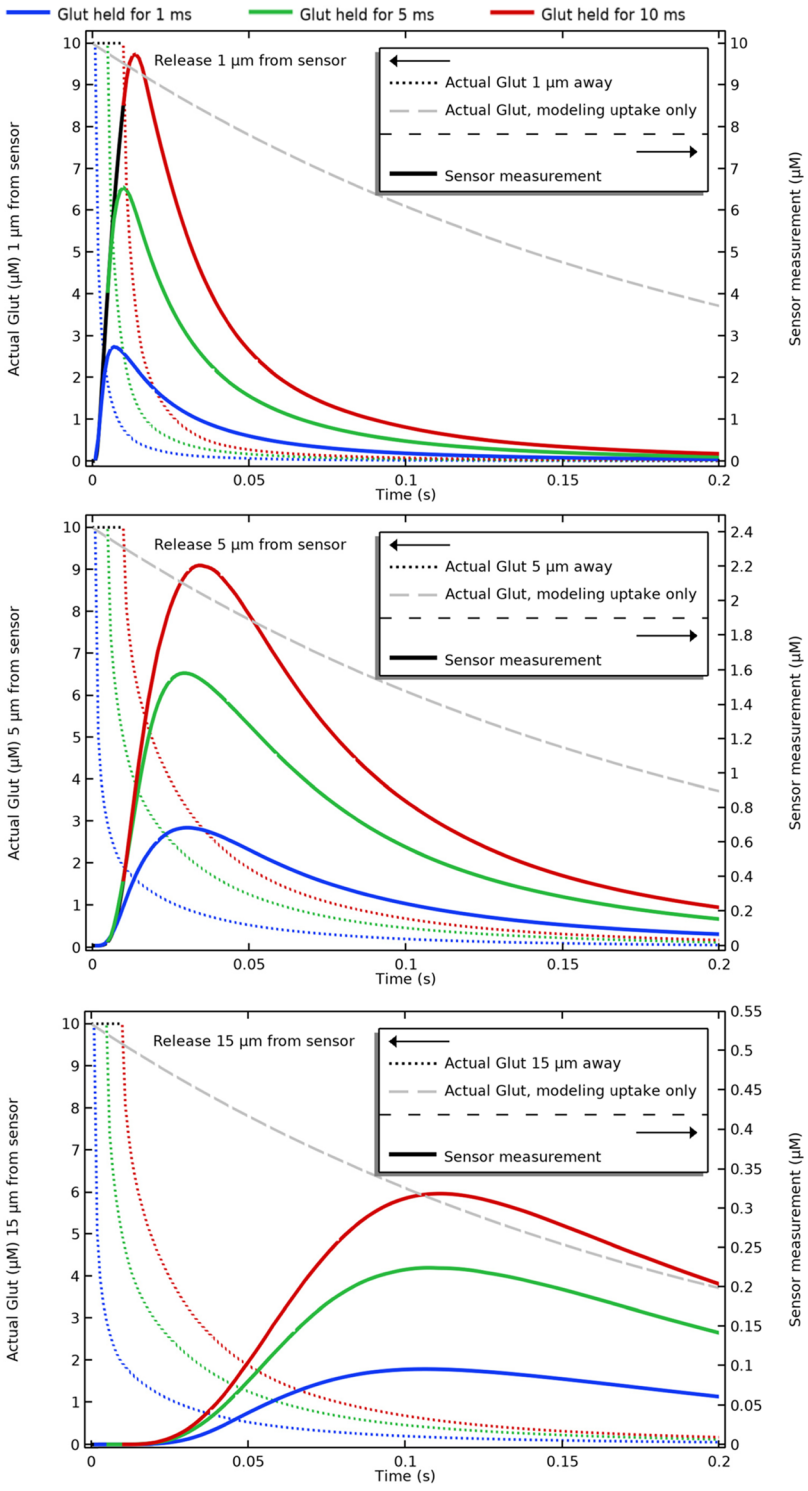

Figure 4. Sensor response to transient Glut release at various distances from a sensor. Solid curves showing simulated sensor responses are to be read using the *y*-axis labels on the right. Black portions of solid curves show the sensor response while Glut is maintained at 10 μM (Note: For release events at 5 and 15 μm, the black portions are covered by the colored curves). Simulations were conducted using the moderate rate constants for Glut uptake (4.95 s^{-1}) and for H_2O_2 clearance (5 s^{-1}). The dotted curves show the actual Glut concentration at the release site. In all plots, the blue, green, and red curves represent data for Glut release times of 1, 5, and 10 ms, respectively. The dashed gray curves (to be read using the *y*-axis on the left) show modeled Glut disappearance due only to an imposed biological uptake corresponding to a 4.95 s^{-1} rate constant (no diffusion and no sensor consumption).

controlling as the distance between the sensor surface and the point of Glut release is increased (Figure 2).

As expected, the overall apparent sensor response time increases almost linearly with distance for simulated Glut release events >5 μm from the sensor. Surprisingly, the opposite trend is shown for the closest Glut release distances. This can be explained by examining the steady-state Glut profiles. At short release distances of less than 3 μm, there is

https://doi.org/10.1021/acschemneuro.1c00365
ACS Chem. Neurosci. 2021, 12, 4275−4285

enough Glut entering the sensor layer to be driven to the Nafion/enzyme layer boundary, where the concentration begins to increase nonlinearly. Any H_2O_2 produced here by the accumulating Glut will have an added mass transfer resistance against diffusing back to the outer edge of the sensor, causing an increased response time. At greater release distances, where Glut is fully consumed before reaching the enzyme/Nafion boundary, more H_2O_2 is produced at the outer edge of the immobilized GlutOx layer where it can diffuse directly into the brain thereby resulting in quicker attainment of steady state.

In considering the distances traveled by diffusing molecules in the brain, it is important to acknowledge how the tortuosity of diffusion paths in the brain ECS impacts apparent or effective diffusivities by increasing relative diffusion distances. The anisotropic nature of the brain also influences mass transport, an effect that has been exploited for creation of detailed maps of neural connections using diffusion-weighted magnetic resonance imaging. For example, the diffusion of water has been shown to be significantly faster in the axial direction of myelinated axons.[27] These differences are often characterized in terms of the fractional anisotropy (FA), relating the magnitude of diffusivity in the primary, axial (faster) to radial (slower) directions. In studies of brains of developing Sprague Dawley rats, FA stabilized through developmental cycles to a value of about 0.3.[28] This value corresponds to diffusion in the axial direction that is 1.67 times the average and diffusion in radial directions 0.67 times the average value (assuming equal diffusivities in all radial directions). This could increase or decrease the distance at which sensors can detect Glut depending on where the probe is located within the brain and could prove to be an important factor in deciding where to implant sensors. Also, it is known that glial scarring develops around implants over time unless measures are taken to attenuate it,[29] and such scar tissue likely has different mass transfer properties from normal brain tissue. However, to reduce the complexity of the simulations conducted here while still addressing the main points of discussion, the brain medium is assumed to be isotropic with a void fraction of 0.2 and a tortuosity of 1.6, as mentioned in the Methods.[16]

Although the Glut step change modeled in these initial simulations may not be realistic biologically, these results highlight the impact on the sensor response of the dramatically different conditions used for calibrations in vitro and expected in vivo. Additional simulations described below of the sensor response in vivo to transient Glut release events provide further indication that calibration plots and response time measurements obtained by the typical means in vitro cannot be used straightforwardly for the interpretation of sensor data gathered in vivo.

2.2. Simulated Sensor Response to Transient Glut Release Events at Fixed Distances in the Brain ECS. Figure 2 shows that if Glut concentrations are not maintained at the site of release for >0.09 s, steady-state sensor responses will not be reached for the conditions explored, and the device will provide a signal corresponding to a lower Glut concentration, except for release events within a few microns of the sensor surface. Because it is unlikely that Glut concentration transients corresponding to synaptic events occur on such lengthy time scales, such release events will not be described well by the duration or magnitude (based on calibrations in vitro) of sensor responses. Figure 4 shows simulations of the ideal, optimized sensor response if Glut concentration is held constant at specific distances from the device for short time periods (1−10 ms). This scenario corresponds to a rectangular Glut concentration pulse in time at a point location (Figure 1b). This study is intended to investigate how closely a sensor signal time course might be expected to describe a clearly defined, transient pulse in Glut concentration in a simulated ECS environment. The specific release times investigated (1, 5, and 10 ms) are intended to approximate in vivo timescales. For example, recordings from the rat nucleus accumbens corresponded to exocytosis events with apparent submillisecond rise times and ms decay times, which would result in Glut presence near the synapse over the range of 1−5 ms.[30] As expected, simulated sensor responses to 10 μM Glut concentration releases are shown to vary significantly depending on how long the concentration is maintained and the distance between the sensor and the point of release (Figure 4). Sensor current signals generally correspond to significant underestimates of the actual 10 μM Glut release concentration, except for release events of longer duration within a few microns of the sensor, which is consistent with the simulation results illustrated in Figure 2 for step changes in Glut concentration at varied separations from the sensing site.

It is also notable that although all simulated sensor responses shown in Figure 4 have a similar asymmetric shape, more distant Glut release events result in broader signals with a more extended period of decline. The decay rate of sensor responses has been used by some to estimate extracellular Glut residence times and cellular uptake rates. However, comparisons of the simulated sensor signal decay profiles with the actual declines in Glut concentration at the release point and with the simulated component of Glut concentration drop-off solely because of biological uptake from the ECS (Figure 4) show how difficult it would be to determine such Glut uptake rates directly from signal decay data. The declining sensor signal results from a combination of Glut uptake from the ECS, actual Glut consumption by the sensor, and diffusion of Glut away from the release site. Among these influences, the effect of the sensor is minor but can be observed by comparing the time profiles of actual Glut concentration (the dotted curves in Figure 4) for the three different Glut release distances from the sensor. For release at 1 μm, the Glut concentration decays most quickly; however, at 5 and 15 μm (the more realistic scenarios), the Glut time courses are slower and nearly indistinguishable indicating that consumption of Glut by the sensor has become inconsequential.

Of course, simulation of Glut release in this way lumps together the many factors that actually influence Glut release and concentration regulation in the ECS. These factors may include variations in the number of vesicles releasing Glut during signaling events, the number of molecules contained in each vesicle, the fraction of molecules released by each vesicle, local geometric constraints, unique synaptic structures, the fraction of Glut spillover into the ECS, and even the possibility of Glut release from astrocytes, which has been observed in response to inflammatory conditions[31] that could be caused by probe insertion. After 1, 5, or 10 ms of maintained Glut concentration, there would be approximately 20, 30, or 40 million molecules present locally in the ECS, assuming outward diffusion from a sensor-sized area (a low estimate of the number of molecules). However, because of the 1-D nature of this model, the actual numbers of molecules needed to

https://doi.org/10.1021/acschemneuro.1c00365
ACS Chem. Neurosci. 2021, 12, 4275−4285

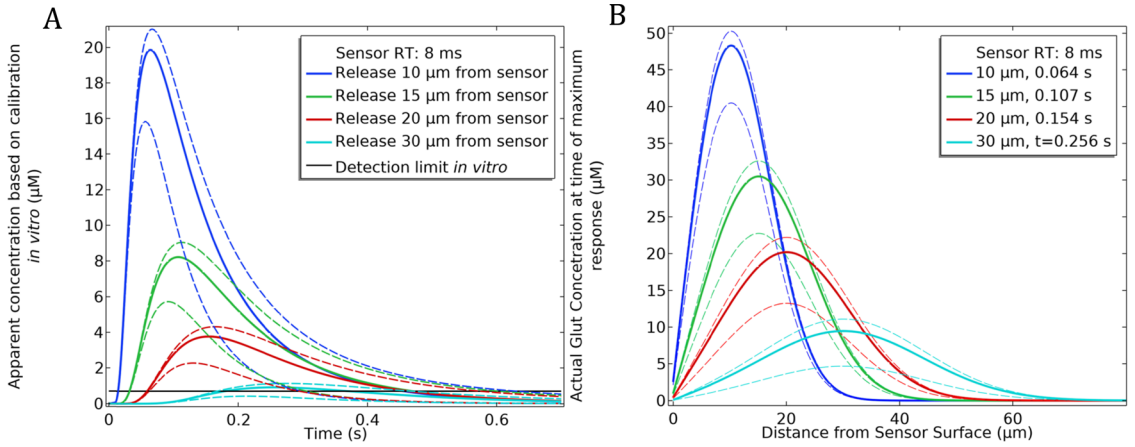

Figure 5. (A) Simulated sensor concentration measurements after bolus releases of Glut at various distances from the sensors within 20 nm, synaptic scale regions, where Glut is specified to be 60 mM at $t = 0$. (B) The actual Glut concentration profiles in the brain plotted versus distance from the sensor surface at the times of maximum sensor response. Dashed curves show the effects of slower and faster uptake or clearance rates of Glut and H_2O_2 corresponding to the lowest and greatest rate constants presented in Table 1, where slower uptake rates result in greater concentrations.

produce these simulated sensor responses would be higher, unless sensor sites are miniaturized significantly. These Glut numbers are still >10−100 times the number found inside a single presynaptic vesicle[32] and do not account for molecules that were taken up from the ECS in those time periods. These 1-D simulations, therefore, should be understood as simplified representations of concurrent release from multiple vesicles and/or synapses.

2.3. Simulated Sensor Response to Bolus Glut Release Events in the Brain ECS. The sensor response also was simulated for single, bolus-type releases of Glut into the ECS at varied distances from the sensor. This simulation roughly represents how these biosensors would respond to neurotransmitter release from synaptic vesicles where it is assumed that vesicles release Glut instantaneously into a volume roughly the size of a synapse, simulated as a 1-D, 20 nm wide region in the ECS, resulting in local concentrations near 60 mM.[33] After release, Glut diffuses through the ECS and the responses of sensors at various distances from the release site were simulated (Figure 5A). The concentrations of Glut within the ECS at the time of the maximum sensor responses also are shown in Figure 5B. The model conditions for these simulations are given in Figure 1c. Simulations corresponding to the extrema of the range of plausible uptake and clearance rates of Glut and H_2O_2 are shown by the dashed curves, although the differences are less pronounced than under the steady-state conditions presented in Figure 2. However as in Figure 2, greater sensor responses are observed for slower clearance and uptake rates, and lower responses are observed when these rates are faster.

At simulated times corresponding to the maximum sensor response, actual concentrations in the brain ECS are much lower than the 60 mM level present initially at the simulated synapse and vary significantly over micron-scale distances (Figure 5B). This observation complicates analysis of how well a sensor reports a bolus release event and the actual concentration in the brain, because the actual Glut profiles show large spatiotemporal variations. It is important to note once again here that the sensor response at any moment is generated from the rate of electrooxidation of H_2O_2 at the Pt electrode surface, which is related directly to the flux of H_2O_2 within the sensor coatings arising from the turnover of Glut by the immobilized GlutOx and the flux of Glut to the sensor surface. As time progresses, the peak Glut concentration diminishes because of Glut diffusion into the simulated ECS away from the sensor as well as Glut clearance from the ECS, which results in a decreasing Glut flux at the sensor surface and a decay in the signal. The effect of Glut consumption by the sensor on simulated Glut concentrations is minimal, although its impact is reflected in the slight shift in the peak centers away from the original 10, 15, 20, or 30 μm release locations as shown in Figure 5B.

These 1-D simulations make it appear possible to observe single, synaptic releases of Glut. However in such 1-D models, we are assuming that the concentration at the release distance is constant across the sensor surface, yet typical sensor surface dimensions of 40 × 150 μm dwarf the size of a synapse. Thus, this simulation describes the sensor response to a release event that likely is much larger than reality, and the actual sensor response in vivo may be much lower. Also, the apparent Glut concentrations corresponding to sensor signals vary significantly depending on the distance between the sensor and location of Glut release, despite the identical Glut release conditions specified for each sensor/release site separation distance. For Glut released farther from the sensor surface, response is lower and broader. For distances greater than 30 μm, even with the 1-D simplifications that overestimate response, simulated response remains below the limit of detection (LOD), which has been determined experimentally as ∼0.7 μM for such sensors.[15] However, this 1-D simulation cannot provide a quantitative prediction of the maximum sensor/release site separation distance that could give rise to a detectable signal, yet the sensor sampling distance likely is far less than the range for electrophysiological recordings (100−200 μm).[12] On a more optimistic note, the peak broadening effect that occurs with increasing Glut release distance from the sensor suggests that it may be possible to correlate the peak widths or rise times to the location of the Glut source relative to the sensor, although this would require experimental validation and careful consideration of relevant assumptions including the time course of Glut release, the concentration

https://doi.org/10.1021/acschemneuro.1c00365
ACS Chem. Neurosci. 2021, 12, 4275−4285

achieved in the synapse, and the Glut leakage rate from the synapse.

It is suspected that in reality only a fraction of the neurotransmitters are released during exocytosis,[34] which would reduce the initial Glut concentration and simulated sensor signals, although not enough is known to account quantitatively for partial neurotransmitter release. This consideration, along with the 1-D nature of the model, further suggests that the simulations likely overestimate the sensor signal and that these results should be understood as maximum possible sensor responses. Nevertheless, these simulation results qualitatively agree with experimental measurements made with less-than-optimal versions of these sensors that had response times in vitro of ∼0.8 s. In the basolateral amygdala, similar sensors detected transient increases in extracellular Glut of ∼1 μM in the time surrounding reward-seeking decisions with release frequencies observed on the order of 1 to 8 per second, depending on rat activity;[35] this is consistent with the observable (above the LOD) rise times of Figure 5A and is within the bounds of the expected response. Another study entailed injection of nanoliter volumes of 500 μM Glut at ∼100 μm from the sensor surface, resulting in a signal corresponding to ∼25% of that expected based on sensor calibration in vitro with signal decay occurring over 3−5 s.[36] Amplitude, rise time, signal decay, and asymmetric signal response in all these cases are consistent with the simulations shown here corresponding to Glut release >20 μm from the sensor surface.

3. METHODS

3.1. Models and Simulation Methods. Mathematical models are used to simulate diffusion and reaction of the three chemical species of primary interest in modeling Glut biosensor performance in vivo: Glut, O_2, and H_2O_2.[21] These processes are described by separate time-dependent mass balance equations for each chemical species in each coating layer of the biosensor (Figure 1) as well as in the brain ECS (four separately defined domains, each described by three linked partial differential equations corresponding to the three species of interest, as seen for the ECS in eq 1). The equations used to describe the biosensor, in one spatial dimension (eq 2), were reported in earlier work.[15,21] In these models, Glut is excluded from the negatively charged Nafion layer using a large partition coefficient of 1000, with equal fluxes and concentrations for all species at all other internal (within the sensor layer) boundaries. Others have published a 1-D model of species diffusion and reaction in the brain ECS suitable for our purposes,[16]

$$\epsilon_b \frac{\delta C_i}{\delta t} = \frac{\epsilon_b}{\lambda^2} D_i \frac{\delta^2 C_i}{\delta x^2} - \epsilon_b r_{i,b}(C_i) \quad (1)$$

i = Glut, H_2O_2, O_2

$$\epsilon_j \frac{\delta C_i}{\delta t} = \alpha_j D_i \frac{\delta^2 C_i}{\delta x^2} + r_{i,j}(C_i) \quad (2)$$

i = Glut, H_2O_2, and O_2; j = PPD, Nafion, and enzyme

In this model, brain porosity and tortuosity of diffusion paths in the ECS are represented by ϵ_b and λ, respectively. As discussed earlier, the assumption of constant diffusivity in anisotropic, heterogeneous brain tissue constitutes a significant approximation. The concentration of species i within the ECS or sensor coating is C_i; its molecular diffusivity in water is D_i; its first-order clearance rate from the ECS is $r_{i,b}(C_i)$ (see Table 1); and the other variables of eq 2 remain consistent with prior models: ϵ_j is the void fraction within sensor coating j; α_j modifies the diffusion coefficient to represent the effective diffusivity; and $r_{i,j}(C_i)$ specifies Glut oxidase enzyme activity in the enzyme layer, which is zero in the other coatings.

Boundary and initial conditions for the brain ECS varied depending on the simulation being performed. A general visualization of the 1-D domains and simulation initial conditions are provided in Figure 1. In all simulations, equal diffusive fluxes for the ECS domain at the sensor immobilized enzyme layer/ECS boundary were specified, using eq 3, where $\alpha_e D_i$ represents the effective diffusivity in the enzyme layer of species i.

$$\frac{\epsilon_b}{\lambda^2} D_i \frac{\delta C_{i,b}}{\delta x} = \alpha_e D_i \frac{\delta C_{i,e}}{\delta x} \quad (3)$$

Also, at the immobilized enzyme layer/ECS boundary, concentrations on either side of the interface were set equal (no concentration partition was specified between these domains). At the edge of the ECS far from the sensor, Glut and H_2O_2 were set at 0 μM, while O_2 was set to a bulk in vivo concentration of 25 μM (see below). To ensure that this boundary condition did not influence simulation results, the length of the ECS domain was increased until further increases did not affect simulation results. To simulate Glut being held at 10 μM for specified time periods, first a constant concentration boundary condition was used for the given time period, then it was removed, and finally, the simulation was continued using data from the last time point.

Solutions to these sets of equations and boundary conditions were generated numerically using COMSOL Multiphysics (COMSOL, Inc, Los Angeles). Equations were entered using the coefficient-form PDE interface. At internal domain boundaries, it was necessary to select the "apply reaction terms on individual dependent variables" option to ensure boundary conditions remained as specified. Time-dependent solutions were found using the default, fully coupled, multifrontal, massively parallel sparse direct solver. Time steps and variable tolerances were adjusted as necessary, depending on the simulation.

A number of assumptions are implicit in these models. In using Fick's Law to construct the diffusion equations, it is assumed that all regions have a homogeneous nature and that concentrations are low. Other assumptions used previously concerning the sensors also apply,[21] including the application of free-enzyme kinetic rate constants for immobilized enzyme, no loss in GlutOx activity upon immobilization and over time, and the nonparticipation of the ammonia byproduct in the reactions of interest. The fraction of active GlutOx in the enzyme layer is assumed to be 0.1, based on the fitting of in vitro experimental data.[15]

3.2. Selection of H_2O_2 Clearance, Glut Uptake, and O_2 Bulk Concentration Parameters. It is assumed that appropriate ranges of rate constants for Glut uptake and for H_2O_2 clearance from the brain ECS can be used to encompass the spectrum of conditions expected, making the model more widely applicable over different regions of the brain. The clearance rates of H_2O_2 and Glut from the brain ECS can greatly affect the simulated sensor response in vivo and are expected to vary depending on many biological factors including differences because of anisotropy, location within the brain, glial scarring around an implanted sensor, and the influence of other neurotransmitters and neuromodulators. These considerations led to the performance of multiple simulations for each set of Glut release conditions to explore a representative range of H_2O_2 and Glut clearance rates described as fast, moderate, and slow in the discussion of simulation results (see Table 1). Further considerations that must be made when interpreting these results concern the possibility of tissue damage resulting from probe insertion,[37] which likely would affect the rates of clearance and uptake. Also if a blood vessel is ruptured on insertion, a layer of red blood cells would be expected to accumulate on the sensor surface,[37] which would alter sensor function. Abnormal accumulation of glial cells also has been observed near inserted electrode probes.[22] Ultimately, the values for first-order clearance or uptake rates (Table 1) were selected based on available literature data and from observations made from sensor use in vivo over a range of values that should be applicable to most biological conditions.

Prior data gathered in vivo with sensors constructed on microelectrode array (MEA) probes did not show evidence of crosstalk between sensor sites arrayed ∼50 μm apart, suggesting that

https://doi.org/10.1021/acschemneuro.1c00365
ACS Chem. Neurosci. 2021, 12, 4275−4285

any H_2O_2 produced at one site is diluted into or cleared by the surrounding ECS before it can diffuse to an adjacent site at sufficient concentration to give a signal. Simulations were performed to determine the minimum clearance rate required for crosstalk to be absent. For sensor spacings of 40 μm on a MEA probe, a clearance rate constant >5 s^{-1} is required. This is consistent with the rate constant measured for cultured Jurkat T cells of 4.5 s^{-1},[23] and was chosen as the mid-range parameter. An upper bound was found by repeating the simulation assuming that crosstalk would not be observed for a smaller sensor spacing of 20 μm, in this case larger rate constants (>30 s^{-1}) would be required. Studies of cultured neurons and astrocytes displayed slower clearance rates on the order of minutes,[24] leading to specification of a slow rate constant representing a 1-min halftime (0.0116 s^{-1}). Other cell types show similarly slow clearance of H_2O_2, including the red blood cells that may be present in cases of insertion damage. For example, mouse red blood cells have shown a H_2O_2 clearance rate constant of 0.048 s^{-1}.[25] Rates this slow would likely result in significant crosstalk between sensors under sustained Glut exposure, but this value was included as the lower bound that may be accurate situationally for certain instances and locations in the brain.

Clearly, measurement of the extracellular H_2O_2 present during Glut monitoring could help improve sensor accuracy. Furthermore, it is worth mentioning that evoked H_2O_2 has neuromodulatory effects and is known to be produced from additional sources in the brain. For example, electrical stimulation of dopaminergic axons has been shown to prompt release of H_2O_2 as well as neurotransmitters.[38] The possibility of these effects was not incorporated into this model but may be worth consideration. In some cases, they could cause a greater sensor response because of H_2O_2 evoked by neuronal stimulation. The importance of H_2O_2 production and regulation to biosensor accuracy are complex, and the topic deserves further independent study.

The range of Glut uptake rate constants used was taken from data obtained using a genetically encoded Glut sensing fluorescent reporter (SuperGluSnFR) technique in cultured hippocampal neurons, where Glut dynamics were recorded after electrically stimulating neural tissue at different frequencies.[13] Middle, upper, and lower values for Glut uptake rate constants were estimated from this data, where the uptake rate from a single stimulation resulted in the fastest uptake, and repeated, high-frequency stimulations resulted in the moderate and slower uptake rates. These rate constants likely result in overestimates of Glut uptake rate because diffusion is not accounted for in the experimental measurements; however, they provide a good initial set of values for simulations.

Oxygen concentration was fixed in the bulk ECS for all simulations at a level such that it would not influence results, which is a reasonable approximation based on previous sensor simulations showing that O_2 is not limiting unless the concentration of Glut is held constant at a concentration more than triple that of O_2.[21] Because the concentration of O_2 in the brain ranges from 5−50 μM, similar to that expected for Glut,[39] simplifications to ignore oxygen dependency are not expected to influence simulation results.

4. CONCLUSIONS

A mathematical model was developed to simulate the performance in vivo of electroenzymatic Glut sensors, which highlights the complex relationship to calibration in vitro that is dependent on mass transfer in vivo and the local rates of Glut uptake and H_2O_2 clearance from the brain ECS. Ranges of values for the volume-averaged uptake and clearance rate constants for Glut and H_2O_2 were chosen to represent the range of their probable variations, spatially and temporally, in the brain. Rates of H_2O_2 clearance were shown to be most significant in affecting steady-state sensor signals and apparent response times, which implies a need for additional experimental study of H_2O_2 concentration regulation in the brain. Simulations of sensor steady-state responses to a 10 μM step change in vivo showed that apparent sensor concentration measurements (based on calibration factors obtained in vitro) may be more than double the actual concentration for Glut release events very close to the sensor because of H_2O_2 diffusive mass transfer resistance from the sensor surface that is not present during typical sensor calibrations in vitro. However, if Glut release occurs >3 μm from the sensor surface, measured apparent concentrations are likely to be significantly lower than actual Glut concentrations.

Simulations showing sensor responses to transient Glut as a rectangular pulse in time at specified distance from a sensor also showed great dependence of sensor response on both the relative location and duration of Glut release. If Glut concentrations are maintained for <10 ms, sensor measurements (based on calibration data previously gathered in vitro) are not likely to correspond to the higher actual concentration reached in the brain. As the sensor signal decays in time because of a combination of Glut diffusion away from the sensor, Glut consumption by the sensor (a minor contributing factor), and Glut uptake from the ECS, it is clear that rate constants for Glut uptake cannot be estimated straightforwardly from signal decay data. Furthermore, as the distance between the sensor and the Glut release site was increased, the sensor signal became progressively broader and weaker.

For the most biologically relevant simulations performed, in which a bolus Glut release is specified within a 20 nm region at various distances from the sensor, it was shown that detection of Glut release within 30 μm of the sensor is feasible and that the breadth of the sensor response is related to the sensor distance from the release site. This information could be useful in distinguishing Glut release events from various locations using a single sensor if all release events are assumed to have the same character, including magnitude and duration. In situations where measuring the magnitude of Glut release events is of primary importance, it is noted that although the sensor response can be correlated well to a bulk concentration in a well-mixed beaker, there can be a very large spatial variation in Glut concentration local to a sensor within the ECS at the time of peak response that would not be readily apparent when analyzing sensor data.

Electroenzymatic biosensors of similar construction for other biomolecules are expected to be affected similarly by conditions in vivo, especially considering the key importance of H_2O_2 dynamics in the sensor response reported here. Deviations from performance in vitro may even be more pronounced for sensors using different enzymes with slower kinetics, as differences in sensor response time are expected to have a large effect on the ability of simulated sensors to monitor quickly changing concentrations.[21]

Within the context of the available sensing techniques, miniaturization of Glut sensors will be necessary (and is feasible considering recent sensitivity improvements)[15,40] if electroenzymatic sensing techniques are intended to operate with spatiotemporal resolution approaching that of devices for electrophysiological recordings,[41] which have resolved >250 Hz action potentials within ∼50 μm of a three-dimensional electrode array.[42] An approach to similar levels of spatiotemporal resolution with electroenzymatic sensors would provide exciting opportunities for simultaneous electrophysiological and electrochemical recordings and the correlation of chemical signaling with neuronal activity.

The current 1-D model cannot be used to determine the lateral spatial resolution of these electroenzymatic sensors.

https://doi.org/10.1021/acschemneuro.1c00365
ACS Chem. Neurosci. 2021, 12, 4275−4285

However, this 1-D model provides a foundation upon which to construct a 3-D model, to further investigate the spatial resolution issue, and perhaps to optimize overall probe design for improved spatial resolution.

AUTHOR INFORMATION

Corresponding Author

Harold G. Monbouquette − *Chemical and Biomolecular Engineering Department, University of California, Los Angeles, California 90095−1592, United States;* orcid.org/0000-0001-8144-8189; Phone: 310-825-8946; Email: hmonbouq@ucla.edu

Author

Mackenzie Clay − *Chemical and Biomolecular Engineering Department, University of California, Los Angeles, California 90095−1592, United States*

Complete contact information is available at: https://pubs.acs.org/10.1021/acschemneuro.1c00365

Author Contributions

The model was prepared by M.C.; simulations were performed by M.C.; the analysis was performed by M.C. and H.M.; the manuscript was written by M.C. and H.M.; and the study was conceived and supervised by H.M.

Funding

This research was supported by NIH (R01NS087494).

Notes

The authors declare no competing financial interest.

REFERENCES

(1) Weltin, A.; Kieninger, J.; Urban, G. A. Microfabricated, amperometric, enzyme-based biosensors for in vivo applications. *Anal. Bioanal. Chem.* **2016**, *408*, 4503−4521.

(2) Xiao, T. F.; Wu, F.; Hao, J.; Zhang, M. N.; Yu, P.; Mao, L. Q. In Vivo Analysis with Electrochemical Sensors and Biosensors. *Anal. Chem.* **2017**, *89*, 300−313.

(3) Ou, Y. G.; Buchanan, A. M.; Witt, C. E.; Hashemi, P. Frontiers in electrochemical sensors for neurotransmitter detection: towards measuring neurotransmitters as chemical diagnostics for brain disorders. *Anal. Methods-Uk* **2019**, *11*, 2738−2755.

(4) Ganesana, M.; Lee, S. T.; Wang, Y.; Venton, B. J. Analytical Techniques in Neuroscience: Recent Advances in Imaging, Separation, and Electrochemical Methods. *Anal. Chem.* **2017**, *89*, 314−341.

(5) Beamer, E.; Conte, G.; Engel, T. ATP release during seizures - A critical evaluation of the evidence. *Brain Res. Bull.* **2019**, *151*, 65−73.

(6) Kiyatkin, E. A.; Wakabayashi, K. T. Parsing glucose entry into the brain: novel findings obtained with enzyme-based glucose biosensors. *ACS Chem. Nerosci.* **2015**, *6*, 108−116.

(7) Wang, B.; Wen, X.; Cao, Y.; Huang, S.; Lam, H. A.; Liu, T. L.; Chung, P. S.; Monbouquette, H. G.; Chiou, P. Y.; Maidment, N. T. An implantable multifunctional neural microprobe for simultaneous multi-analyte sensing and chemical delivery. *Lab Chip* **2020**, *20*, 1390−1397.

(8) Ngernsutivorakul, T.; Steyer, D. J.; Valenta, A. C.; Kennedy, R. T. In Vivo Chemical Monitoring at High Spatiotemporal Resolution Using Microfabricated Sampling Probes and Droplet-Based Microfluidics Coupled to Mass Spectrometry. *Anal. Chem.* **2018**, *90*, 10943−10950.

(9) Ngernsutivorakul, T.; White, T. S.; Kennedy, R. T. Microfabricated Probes for Studying Brain Chemistry: A Review. *ChemPhysChem* **2018**, *19*, 1128−1142.

(10) Lin, M. Z.; Schnitzer, M. J. Genetically encoded indicators of neuronal activity. *Nat. Neurosci.* **2016**, *19*, 1142−1153.

(11) Clark, H.; Monaghan, J.; Yang, H. R.; Xia, J. F.; Mu, M.; Lovely, A.; Micovic, N. SPARC_A DNA-based optical nanosensor for in vivo imaging of acetylcholine in the peripheral nervous system. *FASEB J.* **2020**, *34*, 1.

(12) Marblestone, A. H.; Zamft, B. M.; Maguire, Y. G.; Shapiro, M. G.; Cybulski, T. R.; Glaser, J. I.; Amodei, D.; Stranges, P. B.; Kalhor, R.; Dalrymple, D. A.; Seo, D.; Alon, E.; Maharbiz, M. M.; Carmena, J. M.; Rabaey, J. M.; Boyden, E. S.; Church, G. M.; Kording, K. P. Physical principles for scalable neural recording. *Front. Comput. Neurosci.* **2013**, *7*, 137.

(13) Marvin, J. S.; Borghuis, B. G.; Tian, L.; Cichon, J.; Harnett, M. T.; Akerboom, J.; Gordus, A.; Renninger, S. L.; Chen, T. W.; Bargmann, C. I.; Orger, M. B.; Schreiter, E. R.; Demb, J. B.; Gan, W. B.; Hires, S. A.; Looger, L. L. An optimized fluorescent probe for visualizing glutamate neurotransmission. *Nat. Methods* **2013**, *10*, 162−170.

(14) Aharoni, D.; Khakh, B. S.; Silva, A. J.; Golshani, P. All the light that we can see: a new era in miniaturized microscopy. *Nat. Methods* **2019**, *16*, 11−13.

(15) Huang, I. W.; Clay, M.; Wang, S.; Guo, Y.; Nie, J.; Monbouquette, H. G. Electroenzymatic glutamate sensing at near the theoretical performance limit. *Analyst* **2020**, *145*, 2602−2611.

(16) Nicholson, C.; Hrabetova, S. Brain Extracellular Space: The Final Frontier of Neuroscience. *Biophys. J.* **2017**, *113*, 2133−2142.

(17) Newton, A. J.; Wall, M. J.; Richardson, M. J. Modeling microelectrode biosensors: free-flow calibration can substantially underestimate tissue concentrations. *J. Neurophysiol.* **2017**, *117*, 937−949.

(18) Wightman, R. M.; Amatorh, C.; Engstrom, R. C.; Hale, P. D.; Kristensen, E. W.; Kuhr, W. G.; May, L. J. Real-time characterization of dopamine overflow and uptake in the rat striatum. *Neuroscience* **1988**, *25*, 513−523.

(19) Walters, S. H.; Taylor, I. M.; Shu, Z.; Michael, A. C. A novel restricted diffusion model of evoked dopamine. *ACS Chem. Nerosci.* **2014**, *5*, 776−783.

(20) Bard, A. J.; Faulkner, L. R., *Electrochemical Methods: Fundamentals and Applications. 2nd ed. ed.*; Wiley: New York, 2001.

(21) Clay, M.; Monbouquette, H. G. A Detailed Model of Electroenzymatic Glutamate Biosensors To Aid in Sensor Optimization and in Applications in Vivo. *ACS Chem. Nerosci.* **2018**, *9*, 241−251.

(22) Moussawi, K.; Riegel, A.; Nair, S.; Kalivas, P. W. Extracellular glutamate: functional compartments operate in different concentration ranges. *Front. Syst. Neurosci.* **2011**, *5*, 94.

(23) Antunes, F.; Cadenas, E. Estimation of H2O2 gradients across biomembranes. *FEBS Lett.* **2000**, *475*, 121−126.

(24) Dringen, R.; Pawlowski, P. G.; Hirrlinger, J. Peroxide detoxification by brain cells. *J. Neurosci. Res.* **2005**, *79*, 157−165.

(25) Wagner, B. A.; Witmer, J. R.; van't Erve, T. J.; Buettner, G. R. An assay for the rate of removal of extracellular hydrogen peroxide by cells. *Redox Biol.* **2013**, *1*, 210−217.

(26) Hohnholt, M. C.; Blumrich, E. M.; Dringen, R. Multiassay analysis of the toxic potential of hydrogen peroxide on cultured neurons. *J. Neurosci. Res.* **2015**, *93*, 1127−1137.

(27) Alexander, A. L.; Lee, J. E.; Lazar, M.; Field, A. S. Diffusion tensor imaging of the brain. *Neurotherapeutics* **2007**, *4*, 316−329.

(28) Huang, H.; Yamamoto, A.; Hossain, M. A.; Younes, L.; Mori, S. Quantitative cortical mapping of fractional anisotropy in developing rat brains. *J. Neurosci.* **2008**, *28*, 1427−1433.

(29) Eles, J. R.; Vazquez, A. L.; Snyder, N. R.; Lagenaur, C.; Murphy, M. C.; Kozai, T. D.; Cui, X. T. Neuroadhesive L1 coating attenuates acute microglial attachment to neural electrodes as revealed by live two-photon microscopy. *Biomaterials* **2017**, *113*, 279−292.

(30) Wang, Y. M.; Mishra, D.; Bergman, J.; Keighron, J. D.; Skibicka, K. P.; Cans, A. S. Ultrafast Glutamate Biosensor Recordings in Brain Slices Reveal Complex Single Exocytosis Transients. *ACS Chem. Nerosci.* **2019**, *10*, 1744−1752.

(31) Vesce, S.; Rossi, D.; Brambilla, L.; Volterra, A. Glutamate release from astrocytes in physiological conditions and in neuro-

degenerative disorders characterized by neuroinflammation. *Int. Rev. Neurobiol.* **2007**, *82*, 57−71.
(32) Ribrault, C.; Sekimoto, K.; Triller, A. From the stochasticity of molecular processes to the variability of synaptic transmission. *Nat. Rev. Neurosci.* **2011**, *12*, 375−387.
(33) Scimemi, A.; Beato, M. Determining the Neurotransmitter Concentration Profile at Active Synapses. *Mol. Neurobiol.* **2009**, *40*, 289−306.
(34) Omiatek, D. M.; Dong, Y.; Heien, M. L.; Ewing, A. G. Only a Fraction of Quantal Content is Released During Exocytosis as Revealed by Electrochemical Cytometry of Secretory Vesicles. *ACS Chem. Nerosci.* **2010**, *1*, 234−245.
(35) Malvaez, M.; Greenfield, V. Y.; Wang, A. S.; Yorita, A. M.; Feng, L. L.; Linker, K. E.; Monbouquette, H. G.; Wassum, K. M. Basolateral amygdala rapid glutamate release encodes an outcome-specific representation vital for reward-predictive cues to selectively invigorate reward-seeking actions. *Sci. Rep.* **2015**, *5*, 12511.
(36) Hamdi, N.; Wang, J. J.; Walker, E.; Maidment, N. T.; Monbouquette, H. G. An electroenzymatic L-glutamate microbiosensor selective against dopamine. *J. Electroanal. Chem.* **2006**, *591*, 33−40.
(37) Jaquins-Gerstl, A.; Michael, A. C. A review of the effects of FSCV and microdialysis measurements on dopamine release in the surrounding tissue. *Analyst* **2015**, *140*, 3696−3708.
(38) Kulagina, N. V.; Michael, A. C. Monitoring hydrogen peroxide in the extracellular space of the brain with amperometric microsensors. *Anal. Chem.* **2003**, *75*, 4875−4881.
(39) Burmeister, J. J.; Davis, V. A.; Quintero, J. E.; Pomerleau, F.; Huettl, P.; Gerhardt, G. A. Glutaraldehyde Cross-Linked Glutamate Oxidase Coated Microelectrode Arrays: Selectivity and Resting Levels of Glutamate in the CNS. *ACS Chem. Nerosci.* **2013**, *4*, 721−728.
(40) Huang, I. W.; Clay, M.; Cao, Y.; Nie, J.; Guo, Y.; Monbouquette, H. G. Electroenzymatic choline sensing at near the theoretical performance limit. *Analyst* **2021**, *146*, 1040−1047.
(41) Hong, G. S.; Lieber, C. M. Novel electrode technologies for neural recordings (vol 20, pg 330, 2019). *Nat. Rev. Neurosci.* **2019**, *20*, 376−376.
(42) Rios, G.; Lubenov, E. V.; Chi, D.; Roukes, M. L.; Siapas, A. G. Nanofabricated Neural Probes for Dense 3-D Recordings of Brain Activity. *Nano Lett.* **2016**, *16*, 6857−6862.

https://doi.org/10.1021/acschemneuro.1c00365
ACS Chem. Neurosci. 2021, 12, 4275−4285